THEORETICAL AND NUMERICAL STUDY ON THE STRENGTHENED STEEL PLATE SHEAR WALLS BY FRP LAMINATES

M. Khazaei-Poul* and F. Nateghi-Alahi

Structural Engineering Research Center. IIEES, Tehran, Iran
m.khazaei@iiees.ac.ir, nateghi @iiees.ac.ir

*Corresponding Author

(Received: November 06, 2011 – Accepted in Revised Form: December 15, 2011)

doi: *10.5829/idosi.ije.2012.25.01c.04*

Abstract In this paper, nonlinear behavior of strengthened steel plate shear walls (SPSWs) by FRP laminates has been investigated both theoretically and numerically. In the first part, a new method, "the composite-plate frame Interaction (C-PFI) method", has been introduced to predict the shear behavior of the composite steel plate shear wall systems (CSPSWs). In the second part, several models of one-story unstiffened and strengthened SPSWs have been simulated using finite element software, all specimens subjected to quasi-static cyclic loading. Comparison between results of FEM method and C-PFI method show that theoretical formulations can well predict nonlinear behavior of CSPSWs. FEM results show that with strengthening infill steel plate on the steel plate shear walls, yield strength, ultimate shear capacity and secant stiffness of SPSWs can be significantly increased. Moreover, in the all strengthened SPSW the amount of cumulative dissipated energy were increased.

Keywords Steel Plate Shear Wall; FRP Laminate; C-PFI Method; Hysteretic; Nonlinear Analysis.

چکیده در این مقاله، رفتار دیوارهای برشی فولادی تقویت شده با الیاف پلی‌مری (FRP) به صورت تحلیلی و نظرینظری مورد بررسی و ارزیابی قرار گرفته است. ابتدا روش اندرکنش-قاب-ورق کامپوزیتی، برای برآورد رفتار غیرخطی دیوارهای برشی فولادی کامپوزیتی ارائه شده است. در ادامه، چند نمونه دیوار برشی فولادی تقویت نشده و تقویت شده با الیاف پلی‌مری در برنامه المان محدود (ANSYS) مدل سازی شد و تحت بارگذاری شبه-استاتیکی (سیکلی) قرار گرفت. مقایسه نتایج حاصل از روش المان محدود و روش نظرینظری نشان می‌دهد که روش نظری توانسته است به خوبی رفتار چند-خطه سیستم دیوار برشی فولادی کامپوزیتی را برآورد کند. همچنین نتایج تحلیل‌های عددی نشان می‌دهد که با تقویت ورق پرکننده در دیوار برشی فولادی، ظرفیت تسلیم، ظرفیت نهایی و سختی سکانت سیستم به طور محسوس افزایش یافته است. علاوه بر آن در تمامی نمونه‌های تقویت شده افزایش جذب انرژی مشاهده شده است.

1. INTRODUCTION

Steel plate shear wall (SPSW) systems have significant advantage over many other systems in terms of cost, substantial ductility, high initial stiffness, speed of construction, and reduction in seismic mass [1]. SPSW system can be used in different configurations, such as stiffened and unstiffened thin steel plates, and composite steel plates. Unstiffened steel plate shear wall is the basis for SPSW systems. This type of web plate has negligible compression strength, and shear buckling occurs at low levels of loading. Lateral loads are resisted through diagonal tension in the web plate. Stiffened web may also be used to increase shear buckling strength. In this type, the strength is a combination of shear buckling strength and additional strength from diagonal tension action [2]. In composite steel plate shear walls (CSPSWs) system, steel web plates can be stiffened by adding concrete on one or both sides of the web plate. Concrete layers can improve load carrying capacity of SPSWs by permitting utilization of the full yield strength of the infill

plate. In addition, shear strength of the concrete is effective to increase capacity of the system [1].

Steel infill plate can be strengthened by adding number of layers of fiber reinforced polymer laminate in both sides. In this type of CSPSW, like unstiffened SPSW systems, strengthened steel plate has negligible compression strength and shear buckling occurs at low levels of loading. FRP laminate layers are effective to increase post buckling strength, and initial and secant stiffness of the system [3].

During last four decades many experimental and numerical research on seismic performance of un-stiffened and strengthened steel plate shear walls have been carried out and these researches lead to better understanding of this lateral load resistant system. Wagner [4] is the first researcher who used a complete and uniform tension fields to determine the shear strength of a panel with rigid flanges and very thin web, and inferred that the shear buckling of a thin aluminum plate supported adequately on its edges does not constitute failure. Other researches were also conducted based on this idea to develop an analytical method for modeling of thin SPSWs. Thorburn et al. [5] developed a simple analytical method to evaluate the shear strength of unstiffened SPSWs with thin steel plates and introduced the strip model to represent the tension field action of a thin steel wall subjected to shear forces. Timler and Kulak [6] modified the formula for the inclination angle of strips with respect to the column using experimental methods. This method has been implemented into the Canadian design codes for steel structures [7] (CAN/CSA 2001) and the AISC (2005b) seismic design specifications [8]. Berman and Bruneau [9] presented plastic analysis method based on the strip models as an alternative for the design of SPSWs. Sabouri-Gohomi et al. [10] proposed plate-frame-interaction (PFI) method to predict the shear behavior of the SPSWs. Astaneh-Asl and Zaho [11-12] performed experimental tests on two specimens of three-story composite shear walls under cyclic loads; both specimens showed highly ductile behavior and stable cyclic post yielding performance. He showed that the concrete layer produces a better distribution of stress in the steel plate, developing tension field lines in a wider region. Lubell et al. [13] tested two single story and one 4-story thin SPSWS under cyclic loading and compared the experimental results with the simplified tension field analytical models and found that the models can predict post-yield strength of the specimens well, with less satisfaction in the elastic stiffness results. Caccese et al. [14] tested five 1/4 scale models of three-story for investigation of the effects of panel slenderness ratio and type of beam-to-column connection. They reported that as the plate thickness increased, the failure mode was governed by column instability and the difference between simple and moment-resisting beam-to-column connection was small. Driver et al. [15] tested a 4-story large-scale steel plate shear wall specimen with unstiffened panels under cyclic loading to determine its behavior under an idealized severe earthquake event. Robert and Sabouri-Gohomi [16] conducted a series of 16 quasi-static loading tests on unstiffened steel plate shear panels with central opening. They recommended that the ultimate strength and stiffness of a perforated panel can be conservatively approximated by applying a linear reduction factor (1-D/d) to the strength and stiffness of a similar solid panel, where D is the hole diameter and d is the specimen width. Vian et al. [17] performed tests on special perforated steel plate shear walls with reduced beam section anchor beams under cyclic loading and reported that the perforated panel reduced the elastic stiffness and overall strength of the specimen by 15% as compared with the solid panel specimen.

In this paper, nonlinear behavior of strengthened steel plate shear walls by FRP laminates has been investigated theoretically and numerically. In the first part, a new method, "the composite-plate frame Interaction (C-PFI) method", has been introduced to predict the shear behavior of the CSPSW systems. In the second part, several models of one-story unstiffened and strengthened SPSWs have been simulated in finite element software (ANSYS), and all specimens are subjected to quasi-static cyclic loading, and the results are presented.

2. SHEAR ANALYSIS OF COMPOSITE STEEL PLATE SHEAR WALL

In this part, a new method, "the composite-plate frame Interaction (C-PFI) method", has been introduced to predict the shear behavior of the

composite steel plate shear wall systems. Theoretical formulas, that are recommended in this section, are developed based on the PFI method (PFI method is developed to predict the shear behavior of the SPSWs [5]). Schematic diagram of shear force–displacement of the CSPSWs based on composite-plate frame interaction (C-PFI) method is presented in Figure 1.

The panel shear force–deformation diagram is obtained by superposition of the composite steel plate and frame force–deformation diagrams, as shown in Figure 1. Based on this new method, effect of FRP laminate on the nonlinear behavior of SPSWs is considered.

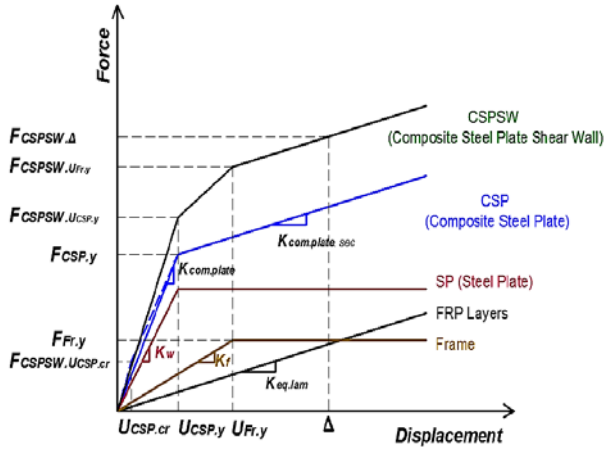

Figure 1. Components of C-PFI model shear force–displacement

2.1. Basic Assumptions In The C-PFI Method The average story of a multi-story structure with SPSWs (Figure 2) can be presented as an isolated panel, for which the following assumptions are made [5].

- Columns are significantly rigid so any deformation would be negligible when calculating shear deflection of the steel plate. It follows that uniform tension field would develop across the entire steel plate.
- The difference in tension-field intensity in adjacent stories is small and therefore bending of the floor beams due to the action of the tension field is neglected.
- The steel plate can be considered as simply supported at its boundaries.
- The effect of stress due to flexural behavior (global bending stresses) on shear buckling stress of the steel plate is neglected.
- The behavior of steel plate and frame are elastic-perfectly-plastic.

With these assumptions, shear behavior of the CSPSW systems can be obtained by superimposing the shear load–displacement diagrams of frame and composite steel plate.

The most common failure mode for FRP-strengthened steel plate is debonding and delamination of the FRP laminate. In theoretical model several assumptions for modeling of FRP layers, bond between steel plate and FRP layer and bond between FRP layers are considered. They are summarized as follows:

- All FRP layers considered have linear elastic behavior and it is assumed that delamination does not occur in the FRP layers.
- A perfect bond is considered at the bond between adhesive and steel infill plate interface and between FRP layers.
- Both fiber reinforced polymer and adhesive in the theoretical model are considered as one layer.
- The adhesive layer is assumed to be thin so that stresses can be considered as constant through the layer's thickness.

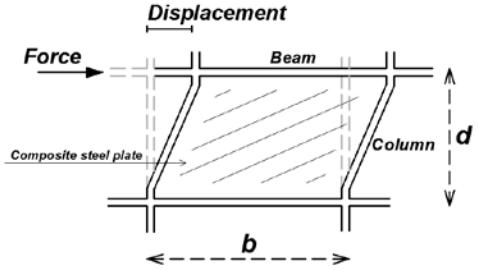

Figure 2. Composite Plate–frame interaction (C-PFI) model plate idealization

2.2. Shear Load–Displacement Diagram of Composite Steel Plate Shear load–displacement of FRP layer only, steel plate only, and composite steel plate only with height d, width b, and thickness t is shown in Figure 3. Behavior of the FRP layers is assumed approximately linear until failure

and steel plate has elastic-perfectly-plastic behavior.

In this Figure, point A corresponds to the buckling limit of the composite steel plate, and point B corresponds to the yielding point of the steel plate in composite steel plate, and point C corresponds to displacements larger than displacement of point B, where steel plate is yielded. Following equations are used to calculate these points.

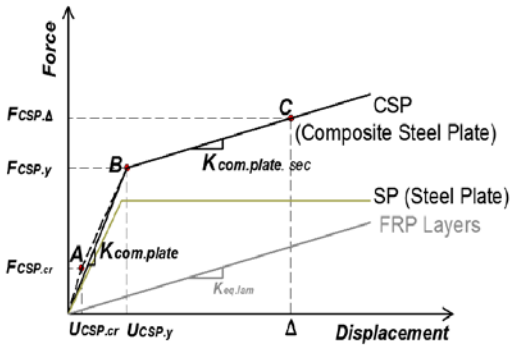

Figure 3. Shear load–displacement of composite steel plate only

2.2.1. Critical Shear Force and Displacement of Composite Steel Plate The elastic critical buckling shear stress, for asteel plate experiencing elastic critical buckling, is calculated as follows:

$$\tau_{cr} = \frac{\pi^2 . E.K}{12.(1-\upsilon^2)} . \left(\frac{t_{st}}{b}\right)^2 \leq \frac{F_y}{3} \qquad (1)$$

where t_{st}, E, K, υ, τ_{cr}, and F_y represent steel plate thickness, elasticity modulus, shear buckling coefficient, Poisson's ratio, elastic critical buckling shear stress of the steel plate, and uni-axial yield stress, respectively. *K* is obtained from (Timoshenko and Goodier 1970) [10]:

$$\begin{cases} k = 5.35 + 4.\left(\frac{b}{d}\right)^2 & \left(\frac{b}{d}\right) \geq 1 \qquad (2) \\ k = 4 + 5.35.\left(\frac{b}{d}\right)^2 & \left(\frac{b}{d}\right) \leq 1 \qquad (3) \end{cases}$$

If several layers of FRP laminate are attached to the steel plate by epoxy, and with assuming that a perfect bond is considered at the bond between adhesive and steel plate interface and between FRP layers, the elastic critical buckling shear stress value for composite steel plate can be approximately obtained from:

$$\tau_{cr} = \frac{\pi^2 . E_{eq.comp(90+\theta)} .K}{12.(1-\bar{\upsilon}^2)} . \left(\frac{t_{eq.comp}}{b}\right)^2 \qquad (4)$$

where $t_{eq.comp}$, $E_{eq.comp(90+\theta)}$, $\bar{\upsilon}$, and θ represent equivalent composite steel plate thickness, equivalent elasticity modulus of composite steel plate in the direction of $(90+\theta)$, Poisson's ratio of composite steel plate, and inclination angle of tension field (See APPENDIX I), respectively. Equivalent composite steel plate thickness is obtained from:

$$t_{eq.comp} = t_{st} + \sum_{i=1}^{N} \frac{E_{lam(90+\theta)_i}}{E_{st}} . t_{lam_i} \qquad (5)$$

in which $E_{lam(90+\theta)_i}$, E_{st}, t_{lam_i}, t_{st}, and N represent elastic modulus of the i-th FRP laminate layer in the direction of $90+\theta$, elastic modulus of steel plate layer , thickness of i-th FRP laminate layer, thickness of steel plate, and number of FRP laminate layers, respectively. Equivalent elastic modulus of composite steel plate in the direction of $90+\theta$ is obtained from Equation (6), in which α_i represents factor between the strain in i-th layer of fiber laminate and steel plate (Figure 4). The value of α_i based on experimental results [18-19] is between 0.17~1. If a perfect bond is considered between adhesive and steel plate interface and between FRP layers, α_i is equal to 1.

$$E_{eq.comp(90+\theta)} = \frac{\sum_{i=1}^{N} \alpha_i . t_{lam_i} . E_{lam(90+\theta)_i} + t_{st} . E_{st}}{\sum_{i=1}^{N} t_{lam_i} + t_{st}} \qquad (6)$$

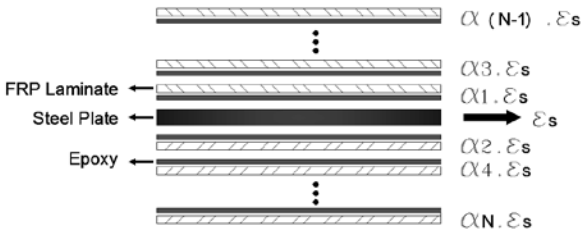

Figure 4. Illustration of the strain symbols in different layers of composite steel plate

From the critical shear stress, the critical shear force of composite steel plate, $F_{CSP.cr}$, is obtained by:

$$F_{CSP.cr} = \tau_{cr}.b.t \quad (7)$$

Limiting elastic displacement of composite steel plate, $U_{CSP.cr}$, is obtained by:

$$U_{CSP.cr} = \frac{\tau_{cr}}{G_{eq}}.d = \frac{\frac{\pi^2.E_{eq.comp(90+\theta)}.K}{12.(1-\upsilon^2)}.\left(\frac{t_{eq.comp}}{b}\right)^2}{G_{eq}}.d \quad (8)$$

In equation (8), G_{eq} is equivalent shear modulus of composite steel plate.

2.2.2. Total Shear Force and Displacement at the Yield of Composite Steel Plate The shear strength of the composite steel plate due to formation of tension field lines, F_{WPb}, in composite steel plate is defined as follows:

$$F_{wpb} = \frac{1}{2}.F_y.b.t_{st}.\sin 2\theta + \sum_{i=1}^{N}\frac{1}{2}.\left(\sigma_{lam_i} = \frac{E_{x'i}}{\alpha_i.E_{st}}F_y\right).b.t_{lam_i}.\sin 2\theta \quad (8)$$

The external work, W_{ext} , of the composite steel plate can be approximately expressed as:

$$W_{ext} = \frac{1}{2}.U_{wpb}.\left(\frac{1}{2}.\sigma_{ty}.b.t_{st}.\sin 2\theta\right) + \sum_{i=1}^{N}\frac{1}{2}.U_{wpb}.\left(\frac{1}{2}.\sigma_{lam_i}.b.t_{lam_i}.\sin 2\theta\right) \quad (9)$$

U_{wpb} is shear displacement of post-buckled component of shear force. The strain energy of the tension strip, W_{int}, considering the effective tension field area can be expressed as:

$$W_{int} = \int \frac{\sigma^2}{2E}t.dA = \frac{\sigma_{ty}^{\ 2}}{2.E_{st}}.b.d.t_{st} + \sum_{i=1}^{N}\frac{\sigma_{lam_i}^{\ 2}}{2.E_{x_i'}}.b.d.t_{lam_i} \quad (10)$$

Shear displacement of the post-buckled component of the shear forces defined as follows. By substituting Eqs. (10) and (11) into Eq. (12):

$$W_{ext} = W_{int} \rightarrow \quad (11)$$

$$U_{wpb} = \frac{2.\sigma_{ty}.d}{E_{st}.\sin 2\theta} \times \frac{t_{st} + \sum_{i=1}^{N}\frac{E_{x'i}}{2.\alpha_i^{\ 2}.E_{st}}.t_{lam_i}}{t_{st} + \sum_{i=1}^{N}\frac{E_{x'i}}{\alpha_i^{\ 2}.E_{st}}.t_{lam_i}} \quad (12)$$

The limiting elastic shear displacement, $U_{CSP.cr}$, is:

$$U_{CSP.y} = U_{CSP.cr} + U_{wpb} \quad (13)$$

Finally, limiting elastic shear force of composite steel plate is obtained from:

$$F_{CSP.U_{CSP.y}} = F_{cr} + F_{wpb} = \tau_{cr}.b.t_{st} + C_{m1}.\left(\frac{1}{2}.F_y.b.t_{st}.\sin 2\theta + \sum_{i=1}^{N}\frac{1}{2}.\left(\sigma_{lam_i} = \frac{E_{x'i}}{\alpha_i.E_{st}}F_y\right).b.t_{lam_i}.\sin 2\theta\right) \quad (14)$$

Limiting elastic displacement of composite steel plate is obtained from:

$$U_{CSP.y} = U_{CSP.cr} + U_{wpb} = \frac{\tau_{cr}.d}{G_{eq}} + C_{m2}.\left(\frac{2.\sigma_{ty}.d}{E_{st}.\sin 2\theta} \times \frac{t_{st} + \sum_{i=1}^{N}\frac{E_{x'i}}{2.\alpha_i^{\ 2}.E_{st}}.t_{lam_i}}{t_{st} + \sum_{i=1}^{N}\frac{E_{x'i}}{\alpha_i^{\ 2}.E_{st}}.t_{lam_i}}\right) \quad (15)$$

C_{m1} and C_{m2} are modifying coefficient of the shear strength and modifying coefficient of the yield displacement, respectively. These modifying coefficients (C_{m1} and C_{m2}) depend on different parameters such as column rigidity, beam–column connection type, etc. and in the SPSWs: $0.8 \le C_{m1} \le 1$ and $1 \le C_{m2} \le 1.7$, [10].

2.2.3. Secant Stiffness of Composite Steel Plate After yield of steel plate layer, secant stiffness of composite steel plate is only provided by FRP laminate layers. Stiffness of one layer of FRP laminate layer can be expressed as:

$$K_{FRP.layer_i} = \frac{E_{x_i'}.b.t_{lam_i}.(\sin 2\theta)^2}{4.d} \quad (16)$$

In which E_{X_i}' is elasticity modules of i-th layer of the FRP laminate layers in the direction of tension field lines. Equivalent stiffness of the composite steel plate, $K_{comp.plate.sec}$, is calculated as:

$$K_{comp.plate.sec} = K_{FRP.layer_1} + K_{FRP.layer_2} + K_{FRP.layer_3} + ... + K_{FRP.layer_N} \quad (17)$$

$$K_{comp.plate.sec} = C_{m3} \cdot \left(\sum_{i=1}^{N} \frac{E_{x_i'}.b.t_{lam_i}.(\sin 2\theta)^2}{4.d} \right) \quad (18)$$

In which C_{m3} is modifying coefficient of the secant stiffness.

2.3. Shear Load–Displacement Diagram of Frame For an internal story of ductile steel plate wall as shown in Figure 5, the shear load–displacement diagram of frame only is shown in Figure 6, [10]. It is assumed here that the beam–column connections are fixed and the beams behave as rigid elements.

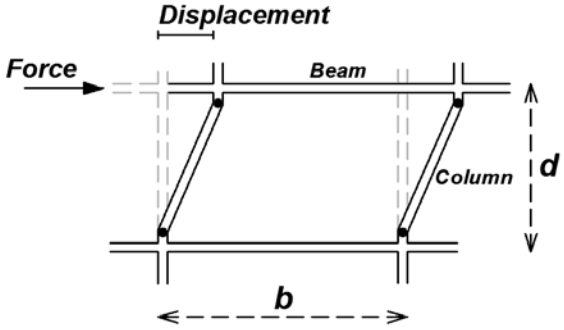

Figure 5. Composite Plate–frame interaction (C-PFI) model plate idealization

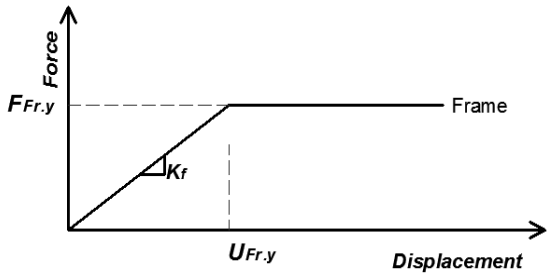

Figure 6. Shear load–displacement of frame only

The shear strength of the frame, F_{Fr_y}, is:

$$F_{Fr_y} = \frac{4.M_{fp}}{d} \quad (19)$$

in which M_{fp} is plastic moment for the column. The limiting elastic shear displacement of the frame, U_{Fr_y}, will be:

$$U_{Fr_y} = \frac{M_{fp}.d^2}{6.E_{st_{fr}}.I_f} \quad (20)$$

in which $E_{st_{fr}}$ and I_f are elastic modulus and moment of inertia of column, respectively. Stiffness of frame, K_{fr}, is obtained from:

$$K_{fr} = \frac{24.E_{st_{fr}}.I_f}{d^3} \quad (21)$$

2.4. Shear Load–Displacement Diagram of CSPSWs In the CSPSWs, shear load–displacement diagram can be obtained by superimposing the shear load–displacement diagrams of frame and composite steel plate as shown in Figure 1. Based on equations presented in previous sections, total shear loads of the CSPSWs is obtained as follows:

1: Total shear force of the CSPSWs, $F_{CSPSW.U_{CSP.cr}}$, at $U_{CSP.cr}$ (corresponding to the buckling limit) is:

$$F_{CSPSW.U_{CSP.cr}} = F_{cr} + K_f \times U_{CSP_{cr}} \quad (22)$$

2: Total shear force of the CSPSWs, $F_{CSPSW.U_{CSP.y}}$, at $U_{CSP.y}$ (corresponding to the yielding point of the steel plate in composite steel plate) is:

$$F_{CSPSW.U_{CSP.y}} = F_{cr} + F_{wpb} + K_f \times U_{CSP.y} \quad (23)$$

3: Total shear force of the CSPSWs, $F_{CSPSW.U_{Fr.y}}$, at U_{fr_y} (corresponding to the yielding point of the frame) is:

$$F_{CSPSW.U_{Fr.y}} = F_{cr} + F_{wpb} + K_{comp.plate.sec} \times \left(U_{Fr.y} - U_{CSP_{cr}}\right) + K_f \times U_{Fr.y} \quad (24)$$

4: Total shear force of the CSPSWs, $F_{CSPSW.D}$, at D (corresponding to displacements larger yielding

point of the frame and composite steel plate) is:

$$F_{CSPSW.\Delta} = F_{cr} + F_{wpb} + K_{comp.plate.sec} \times (\Delta - U_{CSP.y}) + K_f \times U_{Fr.y} \quad (25)$$

In the unstiffened steel plate shear wall, the critical shear strength is insignificant in comparison with post-buckling strength and in such systems, post-buckling tension field action can provide substantial strength, stiffness and ductility. In the strip models, evaluation of the total shear strength in SPSW system is based on post-buckling strength [2]. In the CSPSW systems, like unstiffened SPSW systems, strengthened steel plate has negligible compression strength and shear buckling occurs at low levels of loading. To simplify the equations, the buckling componenet term can be ignored. Therefore, we have:

$$F_{cr} \prec\prec F_{wpb} \Rightarrow F_{CSPy} = F_{wpb} \quad (26)$$

$$U_{cr} \prec\prec U_{wpb} \Rightarrow U_{CSPy} = U_{wpb} \quad (27)$$

3. NUMERICAL STUDY

In this section, seismic behaviour of the CSPSW system have been investigated numerically. In this regard, several models of unstiffened and strengthened SPSW systems in FEM software have been simulated under quasi static loding based ATC-24 and result are presented.

3.1. Basic Assumptions in Numerical Study The most common failure mode for FRP-strengthened steel plate is debonding and delamination of the FRP laminate [18]. In numerical models several assumptions for modeling of FRP layers, bond between steel plate and FRP layer and bond between FRP layers are considered. They are summarized as follows:

- All FRP layers considered are linear elastic.
- Steel materials considered are nonlinear (multi-linear kinematic hardening)
- No slip is allowed at the interface of the bond (a perfect bond is considered at the bond between adhesive and steel infill plate interface and between FRP layers).
- Both a fiber reinforced polymer and adhesive in FEM model are considered as one layer.
- The adhesive layer is assumed to be thin so that stresses can be considered constant through the layers thickness.

3.2 Calibration of he Numerical Models The numerical method has been validated using available experimental results in the literature; therefore, the SPSW1 specimen of Alavi-Nateghi's work [20], Figure 7, is selected and modeled in FEM software (ANSYS-V12). This SPSWs is ½ scaled one-story specimen with around 2 m width and 1.5 m height of unstiffened SPSWs. The boundary elements were similar, while the infill steel plate thickness is 1.5mm. Each specimen consisted of the standard profile HEB160 columns and beams, as boundary elements. At the top of each specimen, an additional HEB160 was placed on the beam and welded along with the flanges, to better anchor the internal panel forces and to contribute with transferring loads of the horizontal jack to the specimen.

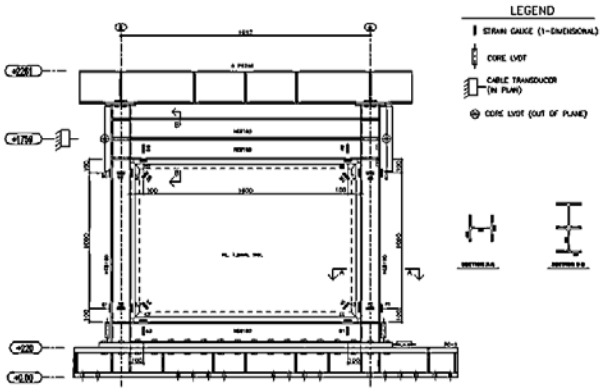

Figure 7. Experimental model of the SPSW1

In our analysis, multi-linear kinematic hardening model is assigned to boundary elements, infill plate, and fish plate. Figure 8 shows the materials model for boundary element, infill plate, and fish plates. Moreover, in this analysis, initial imperfection based on first buckling mode is assigned to the numerical model. The numerical hysteretic and push-over load-displacement curves from the non-linear finite element modeling are presented and compared with experimental model in Figure 9.

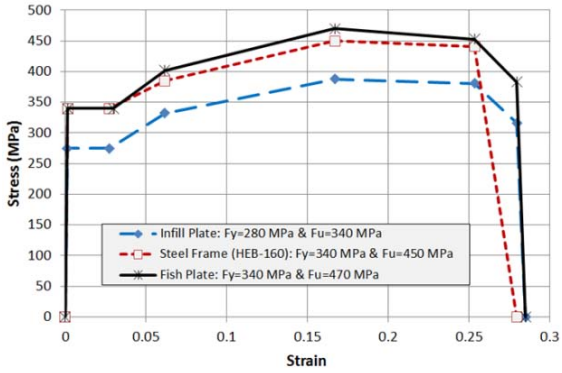

Figure 8. Material models in the SPSW1

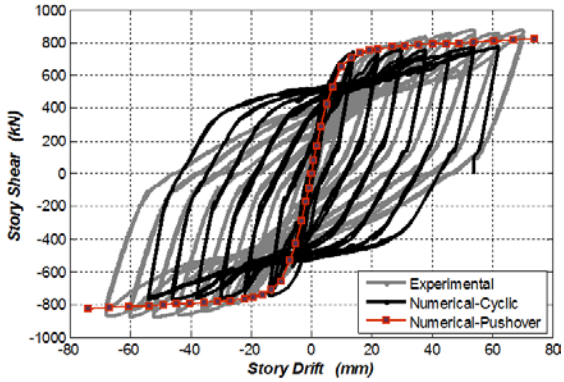

Figure 9. Good agreement between numerical and experimental models

It is obtained that the used numerical method has been successful to estimate the actual shear capacity of the system and initial stiffness of system in comparison with the experimental results. The difference between obtained shear capacity in the numerical and experimental models is less than 5%. The nonlinear results of Von-Mises yield criterion and out-of-plane deformation in 5.4 cm story drift are presented in Figure 10.

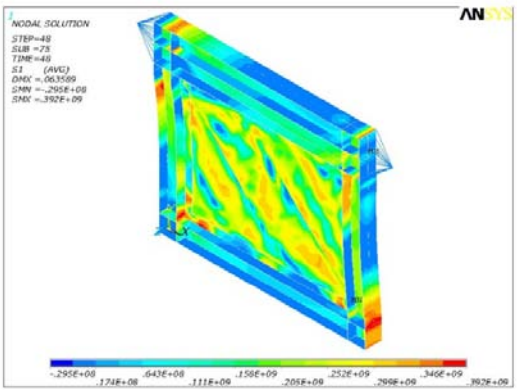

Figure 10. SPSW1,Von-Mises Stresses (Pa.)

3.3 Analysis of Composite Steel Plate Shear Walls In the previous section, verification of the numerical method with an experimental model has been carried out. After verification, infill steel plate in the SPSW1 specimen has been strengthened by numbers of GFRP layers with different orientations of GFRP layers. The methods of arranging the FRP laminates on the infill steel plate are shown in Figure 11.

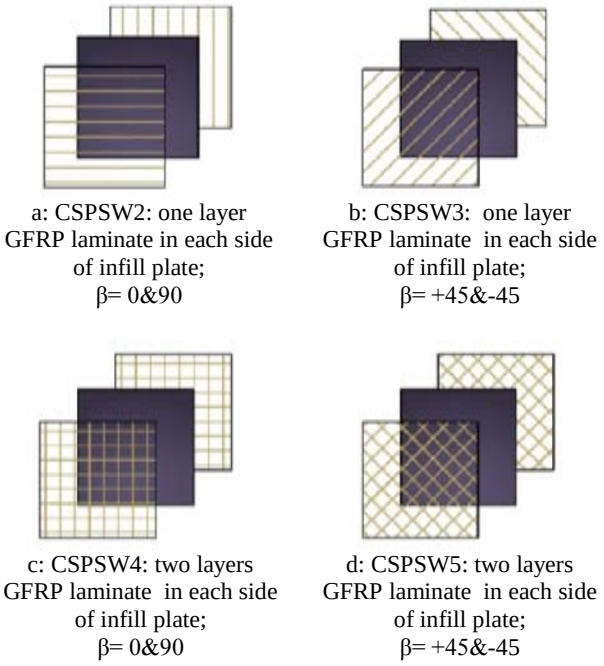

a: CSPSW2: one layer GFRP laminate in each side of infill plate; β= 0&90

b: CSPSW3: one layer GFRP laminate in each side of infill plate; β= +45&-45

c: CSPSW4: two layers GFRP laminate in each side of infill plate; β= 0&90

d: CSPSW5: two layers GFRP laminate in each side of infill plate; β= +45&-45

Figure 11. Different types of strengthening of infill steel plate by GFRP layers

In the CSPSW2 and CSPSW3 specimens, infill steel plate is strengthened by one layer of GFRP laminate on each side, where the GFRP layers are oriented horizontally and vertically (β = 0 & 90) in the CSPSW2 specimen and in a +45 and -45 degrees inclination with respect to the horizontal beam in the CSPSW3 specimens (Figure 11-a,b). In the CSPSW4 and CSPSW5 specimens, infill steel plate are strengthened by two layers of GFRP on each side, where the GFRP layers are oriented horizontally and vertically in the CSPSW4 specimen and in a +45 and -45 degrees inclination with respect to the horizontal beam in the CSPSW5 specimens (Figure 11-c,d). Details of the numerical models are summarized in Table 1.

TABLE 1. Details of the numerical models

Numerical models	Number of layers in composite infill plate		Thickness of laminate and steel plate		Orientation of GFRP	GFRP type
	Steel plate	GFRP layer	Steel plate	GFRP layer		
SPSW1	1	0	1.5 mm	1 mm	-	-
CSPSW2	1	2	1.5 mm	1 mm	0 & 90	SikaWrap® Hex 430G
CSPSW3	1	2	1.5 mm	1 mm	+45 & -45	SikaWrap® Hex 430G
CSPSW4	1	4	1.5 mm	1 mm	0 & 90	SikaWrap® Hex 430G
CSPSW5	1	4	1.5 mm	1 mm	+45 & -45	SikaWrap® Hex 430G

In the finite element models, SHELL-181 is used for modeling of the GFRP layers and infill plate. SHELL181 is a 4-node 3-D element with 6 degrees of freedom at each node. The element has full nonlinear capabilities including large strain and allows defining 255 layers. Shell section is used for modeling composite infill layers (GFRP layers that are attached to infill steel plate). Kinematic hardening plasticity model has been utilized with multi-linear kinematic hardening material model for the mild steel material. The GFRP layers are modeled as an orthotropic material. Mechanical properties of the GFRP laminate, such as young's modules and tensile strength are summarized in Table 2.

Tsai-Wu Failure Criterion, which allows nine failure stresses and three additional coupling coefficients, is assigned to GFRP layers.

TABLE 2. Mechanical properties of GFRP laminate

	Tensile Modulus		Tensile Strength	
GFRP	Ex (MPa)	Ey (MPa)	Tx (MPa)	Ty (MPa)
SikaWrap® Hex 430G	26493	7069	537	23

3.4. Discussion of Numerical Results After verification, the SPSW1 specimen has been strengthened by number of GFRP layers with different orientations. Hysteretic load-displacement curves for the specimens are presented in Figures 12-(a, b, c and d). As shown in this figure, very good hysteretic performance of SPSWs and CSPSWs can be noticed. Ultimate shear strength of the SPSW1, CSPSPW2, CSPSPW3, CSPSPW4, CSPSPW5 are equal to 776 kN, 1012 kN (30% increase in shear strength), 1181 kN (52% increase in shear strength), 1193 kN (54% increase in shear strength) and 1365 kN (76% increase in shear strength), respectively. It can be observed that strengthening by GFRP layers can significantly increase the ultimate shear strength of CSPSWs. Based on numerical results; ultimate strength of CSPSW3 is greater than CSPSW2 and also ultimate strength of CSPSW5 is greater than CSPSW4. These results show that if principal orientation of the GFRP laminate layer lies in the direction of tension field lines, shear capacity of system will be increased.

In Figure 13, the comparison in terms of cumulative dissipated energy of all specimens is provided. Numerical results show that GFRP layers are able to increase cumulative dissipated energy of SPSWs. Based on these numerical results it can find out that actually principal orientation of GFRP layer doesn't have significant effect in the amount of dissipated energy by specimens. In adition, by increasing the number of GFRP layers cumulative dissipated energy is increased.

In Figure 14, the comparisons in terms of secant shear stiffness of all specimens are represented. These numerical results show that GFRP layers increased secant stiffness of steel plate shear walls. Principal orientation of GFRP layer has a significant effect in the amount of secant stiffness of the CSPSW systems. Maximum secant stiffness of the composite SPSWs occurs in the condition that principal orientation of GFRP layers is approximately parallel with tension fields in infill plate.

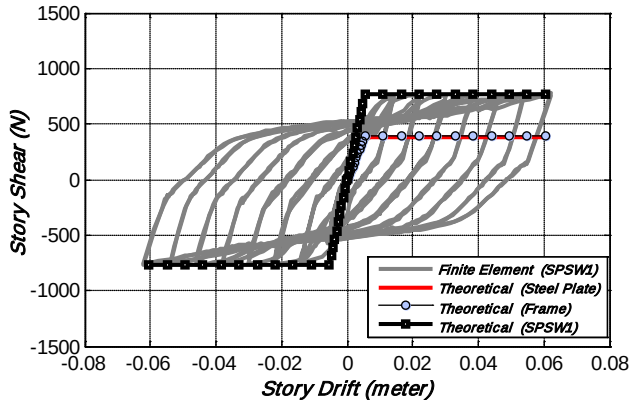

a: SPSW1 specimen

C_{m1}= 1 : C_{m2}=1.65

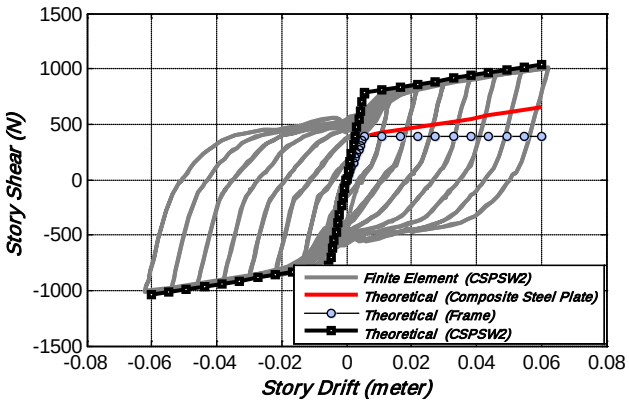

b: CSPSW2 specimen

C_{m1}= 1 : C_{m2}= 1.65 : C_{m3}= 0.9

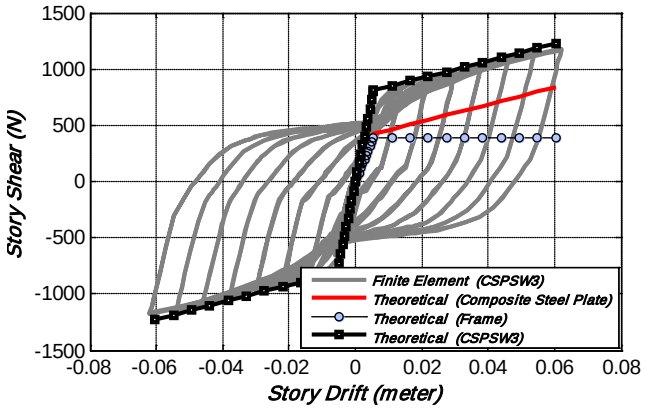

c: CSPSW3 specimen

C_{m1}= 0.9 : C_{m2}= 1.65 : C_{m3}= 0.65

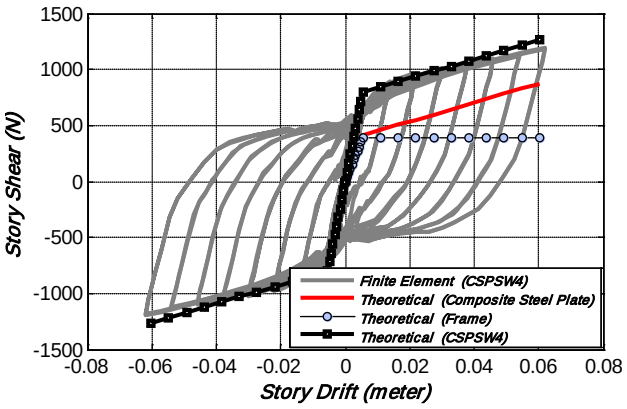

d: CSPSW4 specimen

C_{m1}= 1 : C_{m2}= 1.65 : C_{m3}= 0.8

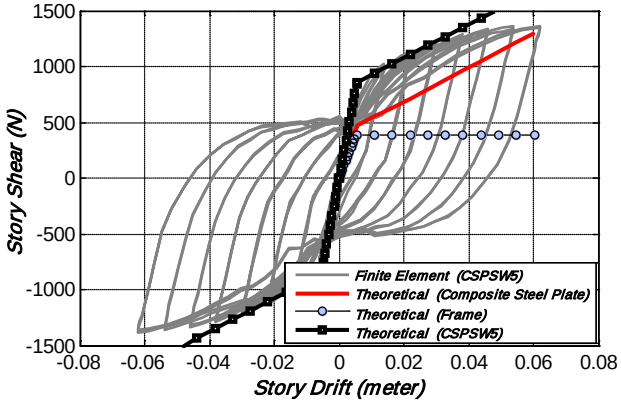

e: CSPSW5 specimen

C_{m1}= 0.9 : C_{m2}= 1.65 : C_{m3}= 0.65

Figure 12. Hysteretic curves of specimens and comparison between finite element results and theoretical method

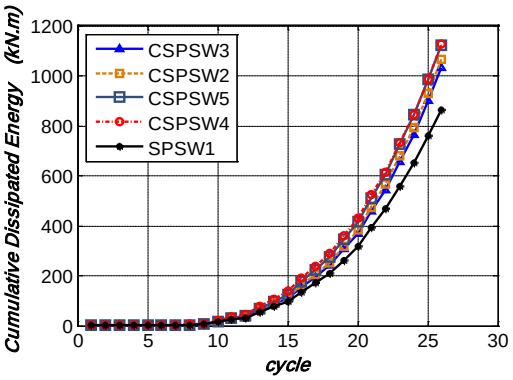

Figure 13. Cumulative dissipated energy of the specimens

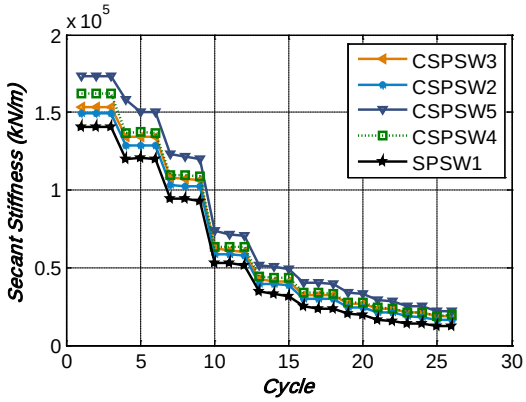

Figure 14. Secant stiffness of the specimens

In Figure 15, the comparison in terms of equivalent viscous damping ratio of all specimens is provided. Numerical results show that by strengthening of the steel infill plate, equivalent viscous damping ratios of system is decreased. The SPSW1 specimen has a maximum equivalent viscose damping ratio amongst all specimens. On the other hand, the CSPSW5 specimen has a minimum equivalent viscous damping ratio between all the specimens. Numerical results show that if principal orientations of the GFRP layers lie in direction of tension field lines, equivalent viscose damping ratio of the CSPSWs will be decreased.

4. COMPARISON BETWEEN FEM RESULTS AND THEORETICAL METHOD

To evaluate the effectiveness of the C-PFI method, the numerical results of strengthened SPSWs are compared with the results of this method. Comparison between finite element results and theoretical method are presented in Figure 12. These results show that theoretical method overcomes to predict multi-linear behaviour of the CSPSW systems approximately. In the CSPSW2 specimen, the C-PFI method fits the results when C_{m1}=1, C_{m2}=1.65 and C_{m3}=0.9 as shown in Figure 11(b). In the CSPSW3 specimen, there is a good agreement between theoretical and FEM results when C_{m1}=0.9, C_{m2}=1.65 and C_{m3}=0.65. In the CSPSW4 and the CSPSW5, modifying coefficients are equal to C_{m1}=1, C_{m2}=1.65, C_{m3}=0.8 and C_{m1}=0.9, C_{m2}=1.65, C_{m3}=0.65, respectively. Based on these results, when $0.9 \leq C_{m1} \leq 1$, C_{m2}=1.65 and $0.65 \leq C_{m3} \leq 0.9$ there is a good agreement between C-PFI method and FEM results.

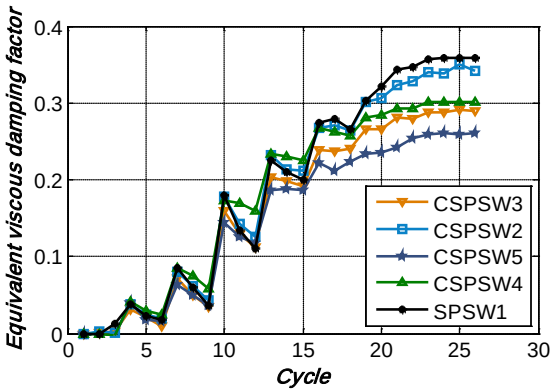

Figure 15. Equivalent viscous damping ratio

5. CONCLUSIONS

In this paper, nonlinear behavior of strengthened steel plate shear walls (SPSWs) by FRP laminates has been investigated theoretically and numerically. The main results can be summarized as follows:

- FEM results show that, with strengthening the infill steel plate, yield strength and ultimate shear capacities of CSPSWs can be significantly increased. In addition to increasing the initial stiffness of the system, after the yielding of the steel infill plate, the system has significant secant stiffness. If principal orientation of GFRP laminate lie in the direction of tension field lines, shear

strength, and secant stiffness of CSPSW system will be increased.

- On the strengthened specimens the amount of absorbed energy increased. Based on these results, it can be inferred that actually the principal orientation of GFRP layers does not have a significant effect on the amount of dissipated energy in the specimens, but adding a number of GFRP laminate layers will increase capability of the system to absorb energy.
- In this paper a simple numerical model, the Composite-Plate Frame Interaction (C-PFI) method, has been introduced, and it has been demonstrated that the method is able to properly predict the shear behavior of the CSPSW systems. Based on comparison between finite element results and theoretical method results, when $0.9 \leq C_{m1} \leq 1$, C_{m2}=1.65 and $0.65 \leq C_{m3} \leq 0.9$ there is a good agreement between C-PFI method and FEM results.

6. APPENDIX

APPENDIX I:

The inclination angle proposed by the Canadian Steel Design Standard (CAN/CSA-S16-01) is as follows [10]:

$$\theta = 90 - \alpha \tag{28}$$

$$\tan^4 \alpha = \frac{\frac{2}{t.b} + \frac{1}{A_c}}{\frac{2}{t.b} + \frac{2.d}{A_b.b} + \frac{d^4}{180.I_f.b^2}} \tag{29}$$

θ = inclination angle
A_c= cross-sectional area of the column
A_b = cross-sectional area of the beam

APPENDIX II:

1- E_D: Dissipated energy in each cycle that is equal to area of loops in each cycle.
2- K_{sec}: Secant stiffness:

$$K_{sec} = \frac{\Delta F}{\Delta L} = \frac{F_{max} - F_{min}}{\Delta_{max} - \Delta_{min}} \tag{30}$$

3- Equivalent viscous damping ratio (ζ):

$$\zeta = \frac{1}{4\pi}\left(\frac{E_D}{E_S}\right) \tag{31}$$

$$Es = \frac{1}{8}(F_{max} - F_{min}) \times (\Delta_{max} - \Delta_{min}) \tag{32}$$

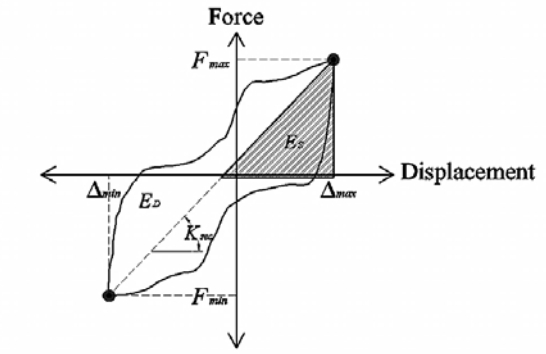

Figure 16. One loop of the hysteretic curves

6. ACKNOWLEDGMENT

The authors would like to gratefully thank the *International Institute of Earthquake Engineering and Seismology (IIEES)* and *Sika-Parsian Co.* for supporting this research.

7. REFERENCES

1. Astaneh- Asl, A., "Seismic Behaviour and Design of Steel Shear walls", Steel TIPS Report, Structural Steel Educational Council, Moraga, CA, (2001).
2. Sabelli, R. and Bruneau, M., "Design Guide 20: Steel Plate Shear Walls", American Institute of Steel Construction, Chicago, IL, USA, (2007).
3. Khazaei-Poul M. and Natghi-Alahi, F., "Behavior of strengthened steel plate shear wall by FRP laminate", M.Sc. Thesis, International Institute of Earthquake Engineering and Seismology, Iran, (2011).
4. Wagner, H., "Flat Sheet Metal Girders with very Thin Webs. Part I. General Theories and Assumptions", Tech Memo. National Advisory Committee for Aeronautics, No. 604, Washington D. C., (1931).
5. Thorburn, L.J., Kulak, G.L. and Montgomery C.J., "Analysis of Steel Plate Shear Walls", Structural Engineering Report. University of Alberta, No. 107, Canada, (1983).
6. Timler, P.A. and Kulak, G.L., "Experimental Study of Steel Plate Shear Walls". Structural Engineering Report, University of Alberta, No. 114, Canada, (1983).
7. CAN/CSA S16-2001, "Limit State Design of Steel Structures", Canadian Standards Association, Willowdale, Canada. (2001).

8. AISC, "Specifications for Structural Steel Buildings", American Institute of Steel Construction, Chicago, IL., USA, (2005b).
9. Berman, J.W. and Bruneau, M., "Plastic analysis and design of steel plate shear walls", ***Journal of Structural Engineering,*** Vol. 129, No. 11, (2003), 1148–1156.
10. Sabouri-Ghomi, V.C. and Kharrazi, H.K., "Shear Analysis and Design of Ductile Steel Plate Walls", ***Journal of Structural Engineering***, Vol. 131, No. 6, (2005).
11. Astaneh-Asl A., "Seismic studies of innovative and traditional composite shear walls", Research project in-progress, Dept of Civil and Env Engineering: Univ. of California, Berkeley, $ Sponsor: National Science Foundation; 1998_2000.
12. Astaneh-Asl A., "Cyclic tests of steel shear walls". Research project. Berkeley: Dept of Civil and Env Engineering, Univ of California; (Sponsor: General Services Administration and Skilling, Ward Magnusson, Barkshire), (2001).
13. Lubell, A.S., Prion, H.G.L., Ventura, C.E. and Rezai, M., "Un-stiffened Steel Plate Shear Wall Performance under Cyclic Loading", ***Journal of Structural Engineering,*** Vol. 126, No. 4, (2000), 453-460.
14. Caccese, V., Elgaaly, M. and Chen, R., "Experimental Study of Thin Steel-Plate Shear Walls Under Cyclic Load", ***ASCE Journal of Structural Engineering,*** Vol. 119, No. 2, (1993), 573-587.
15. Kulak, G.L., Elwi, A.E. and Kennedy, D.J.L. "Cyclic Tests of Four-Story Steel Plate Shear Wall", ***ASCE Journal of Structural Engineering***, (1998), Vol. 124, No. 2, p. 112-120.
16. Sabouri-Ghomi, S. and Roberts, T.M., "Nonlinear Dynamic Analysis of Steel Plate Shear Walls Including Shear and Bending Deformations", ***Engineering Structures***, Vol. 14, No.5, (1992), 309 317.
17. Vian, D., Bruneau, M.K.C. and Tsai, Y.C.L., "Special Perforated Steel Plate Shear Walls with Reduced Beam Section Anchor Beams. I: Experimental Investigation", ***Journal of Structural Engineering***, Vol. 135, No. 3, (2009).
18. Benachour, A., Benyoucef, S., Tounsi, A. and Adda-bedia, E.A., "Interfacial stress analysis of steel beams reinforced with bonded prestressed FRP plate", ***Engineering Structures***, Vol. 30, Issue 11, (2008), 3305-3315.
19. Liu, H.B., Zhao, X.L. and Al-Mahaidi, R., "The effect of fatigue loading on bonding strength of CFRP bonded steel plate joints", ***In: Proceedings of the interna- tional symposium on bond behavior of FRP in structures,*** Hong Kong, China, (2005), 459-464.
20. Alavi, E. and Nateghi, F., "Experimental and Analytical Study on Boundary Elements Effects on Steel Plate Shear Walls Behavior", ***12th Europ. Conf. on Earthq. Eng.***, paper, No. 4, (2010).